UCRL-16058

University of California

Ernest O. Lawrence Radiation Laboratory

ENERGY SPECTRA OF THE $K^+_{\pi 3}$ DECAY MODES

Berkeley, California

DISCLAIMER

UCRL-16058

24
38

UNIVERSITY OF CALIFORNIA

Lawrence Radiation Laboratory
Berkeley, California

Contract No. W-7405-eng-48

ENERGY SPECTRA OF THE $K^{+}_{\pi 3}$ DECAY MODES

Douglas E. Greiner

Ph.D. Thesis

May 15, 1965

ENERGY SPECTRA OF THE $K^+_{\pi 3}$ DECAY MODES

Contents

ENERGY SPECTRA OF THE $K^+_{\pi 3}$ DECAY MODES

Douglas E. Greiner

Lawrence Radiation Laboratory
University of California
Berkeley, California

May 15, 1965

ABSTRACT

Emulsion measurements of the energy spectra of τ'^+ and τ^+ decay are presented. The τ'^+ energy spectrum was measured between 0 and 20 MeV kinetic energy. The energies were determined by range measurements. There were a total of 376 τ'^+ events in this region. If the Q value is known a τ^+ decay is kinematically overdetermined by knowledge of the directions of the momenta of the secondaries. The energies of the 3065 τ^+ events in this sample were determined by this method. It is shown that the density in a Dalitz plot with no charge information is sensitive to nonlinear terms in the square of the matrix element. The τ'^+ decay data were combined with an earlier bubble chamber measurement[3] of the spectrum which covered the region 10 MeV to the maximum allowed energy.

The data from both decays were fitted with a power series parametrization of the matrix element and the Brown and Singer[5] resonance theory. The 0-10 MeV portion of the τ'^+ spectrum was found to deviate markedly from the linear behavior observed above 10 MeV. Thus the low-energy portion of the τ'^+ spectrum is quite sensitive to the resonance hypothesis parameters. The analysis of the τ decay utilized all the information available in the sample by using a maximum likelihood method along with a chi-square analysis to test goodness-of-fit. Previous

analyses of τ decay have used only projections of the Dalitz plot distribution. Results show definite evidence for quadratic terms in the matrix elements of both decays. Best fit "σ" resonance parameters are: τ'^{+} decay $M_\sigma = 345 \pm 5$, $\Gamma_\sigma = 86 \pm 8$; τ^{+} decay $M_\sigma = 348 \pm 2$, $\Gamma_\sigma = 48 \pm 11$. A chi-square test of the resonance hypothesis with the τ^{+} data yields a .4% probability of fit. Although the mass values agree quite well, the disagreement of the width values and the fact that the τ^{+} data is fitted so poorly indicate that the present form of the resonance hypothesis does not provide the correct matrix elements for τ^{+} and τ'^{+} decay.

I. INTRODUCTION

The three body decay reactions

$$K^+ \rightarrow \pi^+ + \pi^+ + \pi^- \qquad (\tau^+ \text{ decay})$$

$$K^+ \rightarrow \pi^o + \pi^o + \pi^+ \qquad (\tau'^+ \text{ decay})$$

have been studied by several experimental groups.[1-4] The matrix elements have been related to the π-π interaction by several authors.[5-8] Relationships between the matrix elements and isotopic spin selection rules have been derived.[9,10] Both matrix elements have been found to vary at least linearly with the energy of the odd pion.

In the case of τ'^+ decay the measurement of the π^+ kinetic energy spectrum by Kalmus et al.[3], made in a heavy liquid bubble chamber, extends from the upper energy limit down to 10 MeV. We have used emulsion to determine the spectrum from 0 to 20 MeV. Combining the two sets of data allows an analysis of the entire distribution.

Earlier measurements of the τ^+ decay energy spectrum have included approximately 500 events.[1,2] By foregoing charge identification we have obtained a sample of 3065 τ^+ events in the same emulsion stack. These τ^+ events are analyzed by a maximum likelihood method which uses all the information available. The increased statistics together with the likelihood analysis provide a sensitive test for the nonlinear contributions to the matrix element.

Experimental details are presented in Section II. Section III presents the experimental data and the results of fits to a power series paramatrization of the matrix element and the "σ" resonance hypothesis. A general discussion of the experiment and a summary of experimental tests of the resonance hypothesis are given in Section IV.

II. EXPERIMENTAL PROCEDURE

A. Exposure and Scanning

A separated beam of positive kaons from the Bevatron was brought to rest in a stack of nuclear emulsion. The stack, shown in Fig. 1, consisted of 250 pellicles of Ilford K.5 emulsion, each pellicle being 600μ thick and 37-by-23-cm. The large stack was designed to assure identification of the long-range $K_{\mu 2}$ decay mode for a branching ratio study. The size of the stack also facilitated $K_{\pi 3}$ decay studies because all such secondaries stopped in the emulsion. The experimental arrangement is shown in Fig. 2. About 2×10^6 kaons entered the stack normal to the plane of the pellicles and came to rest in a 14 cm^3 volume of emulsion centered 13 cm from the upper end. As the stack was dismantled the density of each pellicle was measured and a coordinate grid was printed on the back. Standard processing techniques were used. The minimum grain density achieved was slightly lower than desired; however, minimum ionizing tracks are clearly visible. Each plate had an alignment tab cemented to it along with reinforcement strips to reduce the chance of accidental breakage. The entire stack was aligned to facilitate following tracks from plate to plate. A typical plate is shown in Fig. 3. The coordinate grid is shown in Fig. 4.

All events were located by area scanning. Each scanner had large reproductions of the coordinate grid. All track endings in each millimeter square were examined and the positions of acceptable events were located on the grid-reproduction sheets.

The τ decay mode ($K^+ \rightarrow \pi^-\pi^+\pi^+$) is quite spectacular in emulsion

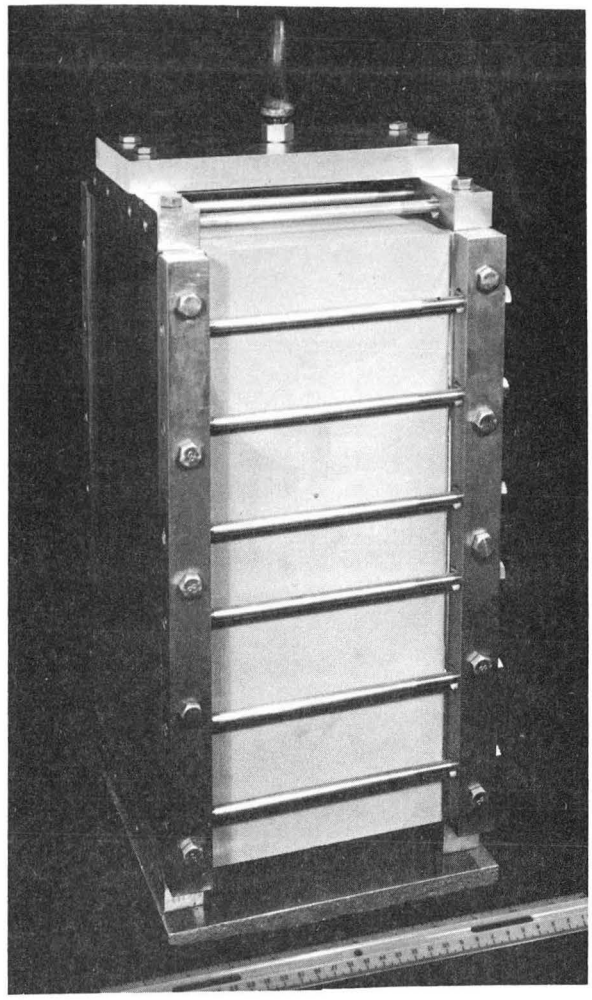

ZN-4969

Fig. 1

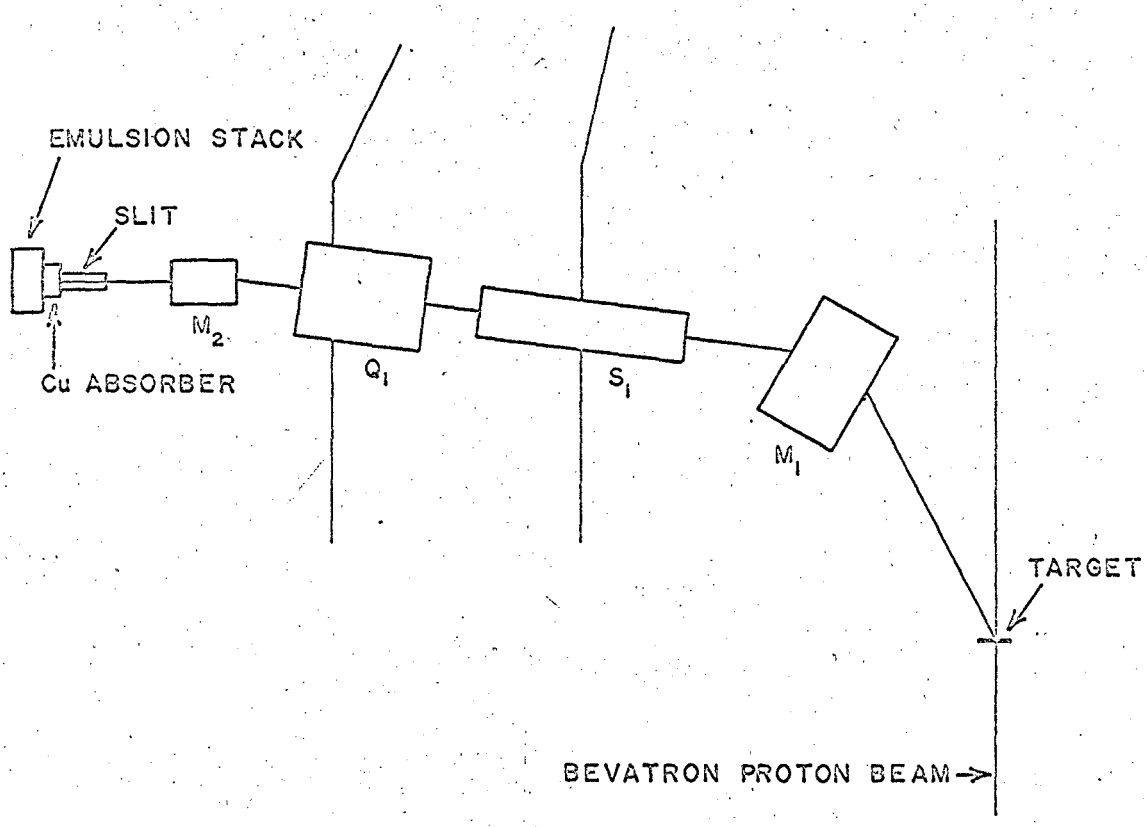
EMULSION STACK
SLIT
Cu ABSORBER
M2
Q1
S1
M1
TARGET
BEVATRON PROTON BEAM

Figure 2

Fig. 3

036 + 091	037 + 091	038 + 091	039 + 091	040 + 091	041 + 091	042 + 091	043 + 091	044 + 091
036 + 092	037 + 092	038 + 092	039 + 092	040 + 092	041 + 092	042 + 092	043 + 092	044 + 092
036 + 093	037 + 093	038 + 093	039 + 093	040 + 093	041 + 093	042 + 093	043 + 093	044 + 093
036 + 094	037 + 094	038 + 094	039 + 094	040 + 094	041 + 094	042 + 094	043 + 094	044 + 094
036 + 095	037 + 095	038 + 095	039 + 095	040 + 095	041 + 095	042 + 095	043 + 095	044 + 095
036 + 096	037 + 096	038 + 096	039 + 096	040 + 096	041 + 096	042 + 096	043 + 096	044 + 096
036 + 097	037 + 097	038 + 097	039 + 097	040 + 097	041 + 097	042 + 097	043 + 097	044 + 097

ZN-4974

Fig. 4

and is easily identified by the presence of three coplanar, charged secondaries with moderate to high grain density. Three prong events can also be produced whenever a neutral pion is a decay product by sequences such as

$$K^+ \rightarrow \mu^+ + \pi^o + \nu$$
$$\qquad\qquad\quad \downarrow \rightarrow e^+ + e^- + \gamma \ .$$

This type of event is rarely coplanar and is usually identifiable by two or more prongs of low grain density. These events, which contain Dalitz pairs, can be expected to contribute about 7.6% of the 3 prong events seen. Other sources of 3 prong events are the rare decay modes K_{e4} and $K_{\mu 4}$. These events again need not be coplanar and in the case of K_{e4} will have at least one minimum ionizing secondary. A few neutron-produced stars may simulate τ decay.

The quality of the sample of τ events depends on the ability to locate 3 prong events and subsequently separate the τ-mode from the rare-mode, Dalitz-pair and neutron-star events. The process of segregating the 3 prong events which are not τ's is described in the section on data reduction.

The efficiency of locating 3 prong events was checked by a complete rescan of the volume used. The appearance of a τ event can vary from a configuration of equal energy secondaries separated by 120° angles to an event with collinear prongs. The decay plane of these events can also appear at any orientation to the emulsion plane. Figure 5 shows several photomicrographs of different τ decay configurations. In order to check for possible scanning bias due to the variety of configurations, efficiencies

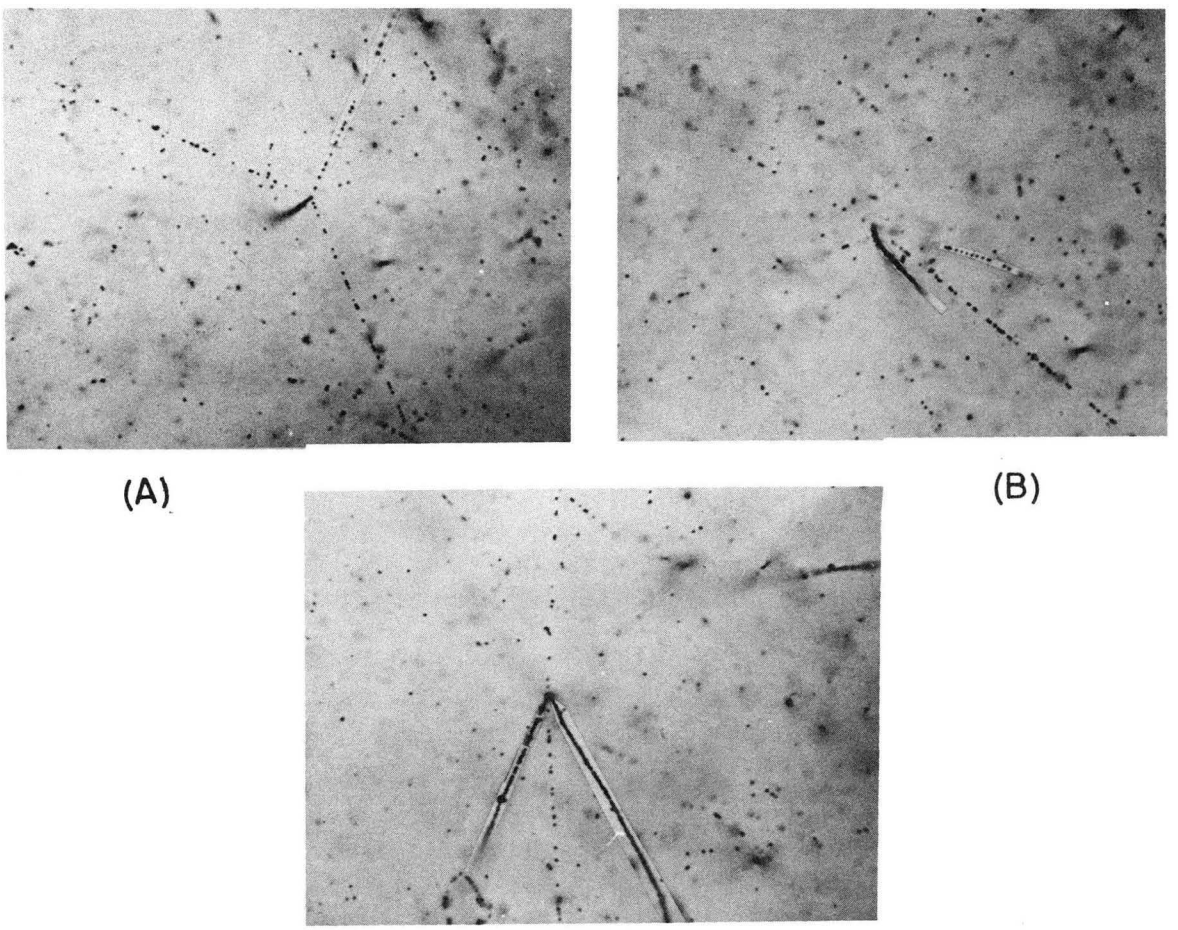

ZN-4975

Fig. 5

were calculated over the distributions of energy of most energetic prong, largest included angle, and direction of the normal to the decay plane. All efficiencies were between 97 and 100% and constant over the distributions. The method of calculating efficiencies and results are given in Appendix A.

The τ' decay mode ($K^+ \to \pi^+\pi^o\pi^o$) appears as a K^+ ending with a single associated secondary of grain density $\geq 1.65 \times$ minimum. Another K^+ decay mode which has this appearance is $K_{\mu 3}$. The grain density of the highest energy τ' secondary is $1.64 \times$ minimum. Both $K_{\pi 2}$ and $K_{\mu 2}$ have grain densities near this (1.2 and 1.05 respectively), and the $K_{\mu 3}$ spectrum covers this range of grain densities also. Thus, measurement of the upper end of the τ' decay spectrum is difficult. However, restricting the measurement to the low energy portion removes the $K_{\pi 2}$ and $K_{\mu 2}$ contamination and greatly reduces the work required. In order to obtain the low energy portion of the τ' energy spectrum, events with a single secondary of ionization $\geq$ twice minimum were recorded--a twice minimum π^+ corresponds to a range of 2.2 cm and a kinetic energy of 37 MeV. The recorded events were then followed. The τ' events were identified by their characteristic $\pi^+ \to \mu^+ \to e^+$ decay sequence. The lower portion of the $K_{\mu 3}$ energy spectrum was unavoidably also obtained and when combined with the $K_{\mu 3}/K_{e3}$ branching ratio provided a determination of the form factor ratio for that decay mode.

Since we are interested here only in the shape of the energy spectrum, the absolute efficiency of τ' detection is not important. What is required is a measure of the relative detection efficiency as a function of energy. The relative efficiency can be defined by considera-

tions of the angular distribution of the π^+ secondaries. This distribution should be isotropic in the absence of scanning bias. In Appendix A the relative efficiency is defined and evaluated. It is found that there is no significant variation of efficiency over the portion of the τ' energy spectrum considered.

B. Measurements and Data Reduction

1. Range Measurement of $\pi^+\pi^o\pi^o$ Mode

The range of each π^+ was measured on a microscope digitized in three mutually perpendicular directions. Each track was split up into straight segments and the coordinates of the endpoints of the segments were punched on IBM cards. The path length in emulsion was calculated with appropriate corrections for shrinkage of the emulsion. The energy was determined from the range energy relation after correction for emulsion density. The accuracy of the energy determined by this method is limited by the range straggling effect which introduces an error of from 1-2%.

2. Angle Measurement of $\pi^-\pi^+\pi^+$ Mode

The direction of each prong of the three prong events was measured by recording the coordinates of two points on each prong with a digitized microscope. If the K rest frame directions of the pions in a τ decay are known then relativistic mechanics supplies us with four equations where, if one assumes knowledge of the kaon and pion masses, only the magnitudes of the three momenta are unknown. Since the problem is overdetermined a fitting program was used to calculate the values of the momenta for each case. The fitting program is quite similar to those used to fit bubble chamber events.[11] A description of the fitting calculation is given in Appendix B.

Several precautions were taken in order to recognize events which were not τ decays:

1. The volume of the parallelepiped formed by unit vectors along the momentum directions was computed. If this volume was greater than .1, the event was remeasured. If the remeasurement also produced a large volume the event was set aside for further analysis. (See Fig. 6.)
2. If the three directions were coplanar they were checked to see if they all pointed to one-half plane. Since it is impossible to balance momenta in this case these events were subjected to further analysis: (See Fig. 6.)
3. All events with chi-square probability less than 1% were further analyzed.
4. All events for which the iteration calculation did not converge were further analyzed.

Further analysis consisted of following the prongs to identify the event. About 10% of the measured events had to be followed. This procedure isolated many Dalitz pair events, five K_{e4} events and one example of the previously unreported $K_{\mu 4}$ decay.[12]

3. Q Value Determination

To provide a check on the above fitting procedure a sample of 47 τ events were followed and range measured. Agreement between the two methods was of the order of 1-2 MeV/c in the momenta of the pions.

The 47 completely analyzed events were also used to determine the Q value of the reaction and hence provide another measurement of the kaon mass. A fitting program was written which used both the angular

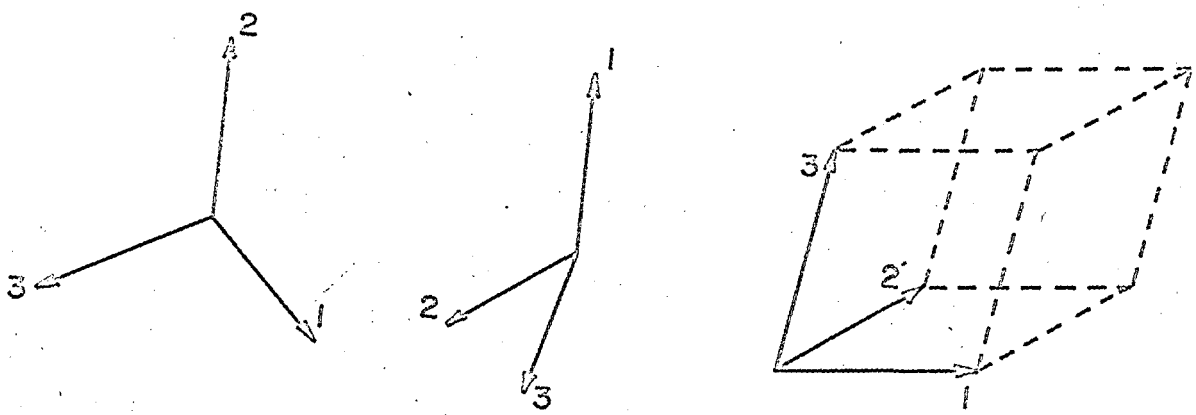

a. b. c.

Figure 6

information and the range information and conservation of 3-momentum to obtain the best energy values for each decay. The resultant kaon mass was (493.8 ± 0.2) MeV which agrees with the accepted value of (493.8 ± 0.2) MeV.[13]

III. RESULTS AND COMPARISON WITH THEORY

The τ' energy spectrum obtained in this experiment is shown in Fig. 10. The 10-20 MeV region was used to normalize our sample to the data of Kalmus et al.[3] and the resultant total spectrum (divided by phase space) is shown in Fig. 7. A chi-square analysis was used to determine the most probable parameters for several types of matrix element. The resultant spectra (computed with best-fit parameters) are also indicated in Fig. 7. The results of the chi-square analysis are given in Table I, while the matrix elements used are shown in Appendix C. Appendix D gives a summary of the statistical methods used to analyze the data.

A look at Table I shows that there is little distinction between a resonance matrix element and a quadratic matrix element while the linear element is a poorer fit.

A maximum likelihood method was used to determine the best-fit parameters to the τ decay Dalitz plot distribution. In order to measure the absolute goodness of fit chi-square calculations were also made.

Since the pion charges are unknown each event can be put on a Dalitz plot in six different ways. Figure 8 shows a Dalitz plot with an event plotted at the six possible points. There is one and only one point per event contained in each of the sextants shown on the figure. Sextant I, where $T_1 \geq T_2 \geq T_3$ was chosen for the fitting calculations.

The density on a Dalitz plot is proportional to the absolute value of the amplitude squared. Let

T_- = kinetic energy of π^-

T_{1+} = kinetic energy of one π^+

TABLE I. Results of τ' analysis.

Matrix element and best fit parameters	χ^2	Number of degrees of freedom	Chi-square probability of fit
Linear Element* $M = 1 + a(s_3 - s_o)$ $a = -.225 \pm .18$	11.98	9	20%
Quadratic Element $M = 1 + a(s_3 - s_o) + b(s_3 - s_o)^2$ $a = -.192 \pm .022$ $b = -.070 \pm .028$	5.84	8	67%
Resonance $M_\sigma = 345 \pm 5$ $\Gamma_\sigma = 86 \pm 8$	5.44	8	71%
Variable Width Resonance $M_\sigma = 351 \pm 5$ $\Gamma_\sigma = 89 \pm 7$	5.44	8	71%

* a is in units of $\frac{1}{M_\pi^2}$, b is in units of $\frac{1}{M_\pi^4}$ and s_3 is the odd-pion Mandelstam variable defined in Appendix C.

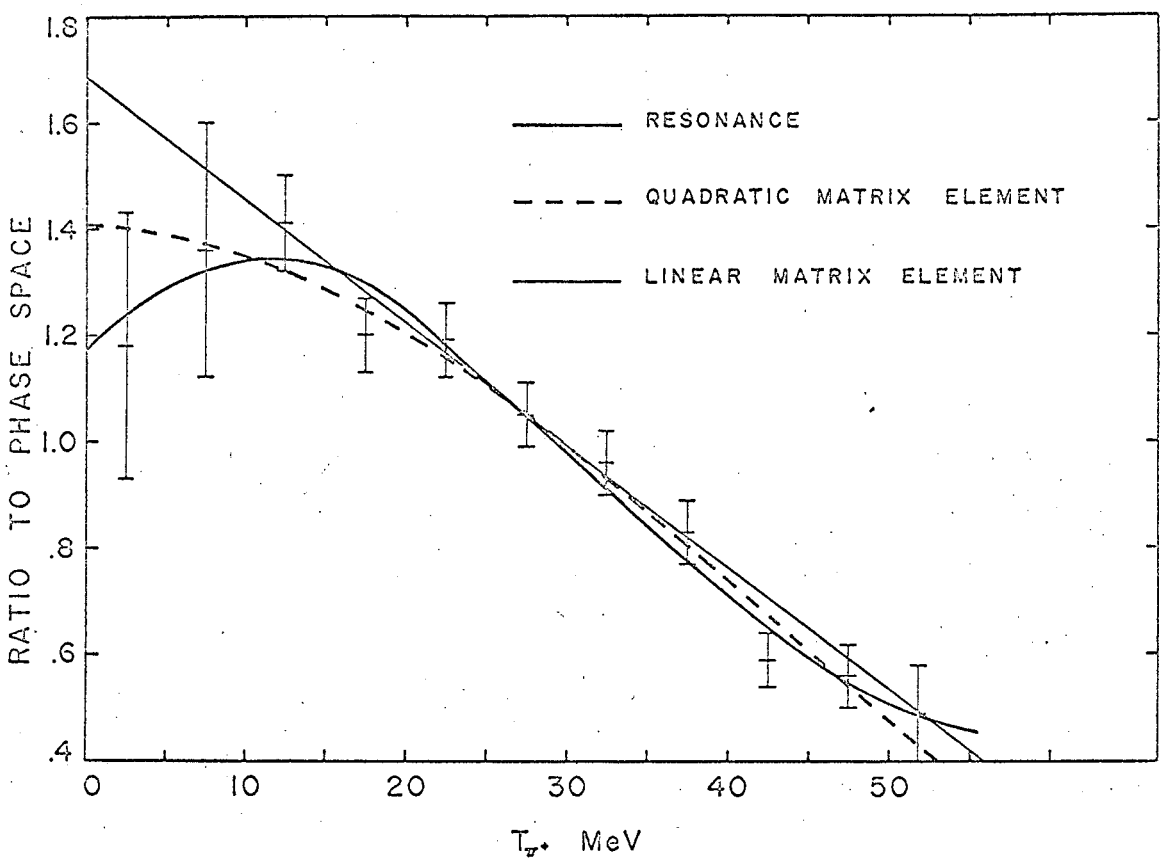
RESONANCE
QUADRATIC MATRIX ELEMENT
LINEAR MATRIX ELEMENT
RATIO TO PHASE SPACE
1.8
1.6
1.4
1.2
1.0
.8
.6
.4
0
10
20
30
40
50
T_{π^+} MeV

Figure 7

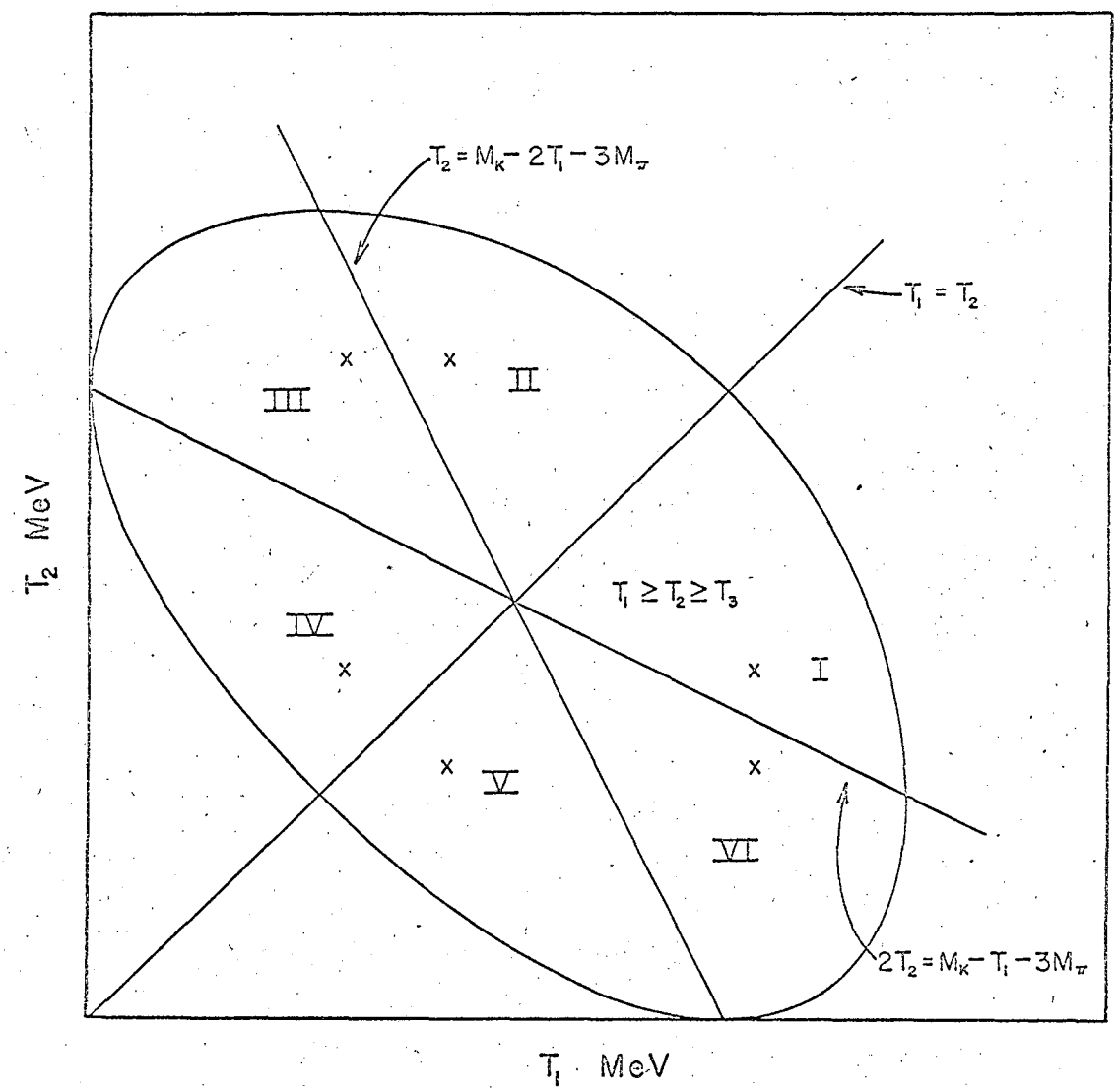
$T_2 = M_K - 2T_1 - 3M_\pi$
$T_1 = T_2$
III
II
$T_1 \geq T_2 \geq T_3$
IV
I
V
VI
$2T_2 = M_K - T_1 - 3M_\pi$
T_2 MeV
T_1 MeV

Figure 8

T_{2+} = kinetic energy of second π^+

In general the density may be written as a function of all three energies (although only two energies are independent)

$$\rho = \rho(T_-, T_{1+}, T_{2+}) .$$

If the charges are not known the density is proportional to the sum over all possible permutations of the charges.

$$\rho \propto \rho(T_-, T_{1+}, T_{2+}) + \rho(T_{2+}, T_-, T_{1+}) + \rho(T_{1+}, T_{2+}, T_-)$$

Here permutations of the type $T_{1+} \rightarrow T_{2+}$ are ignored due to Bose statistics. The density in sextant I of the Dalitz plot was calculated in this manner. The matrix elements used are described in Appendix C.

In order to present the data in a form which will be both compact and useful for future analysis the sextant has been partitioned by a grid including 20 divisions in each direction. Figure 9 shows the sextant with the number of events indicated in each grid. Chi-square minimization calculations using this grid and maximum likelihood calculations using the individual events give best-fit parameters which agree to within the computed errors.

It is shown in Appendix C that, for a matrix element $M = 1 + a(s_3-s_o) + b(s_3-s_o)^2 + c(s_1-s_o)(s_2-s_o)$, keeping quadratic terms in s_i in the density allows us to determine the combinations of coefficients $2b + a^2$ and c. However, it was found that including the 2c term in the density provided no better fit than with only the term whose coefficient is $a^2 + 2b$. Therefore we have assumed the 2c term is not needed. Table II gives the results of maximum likelihood calculations plus a chi-square fit to the resonance hyopthesis.

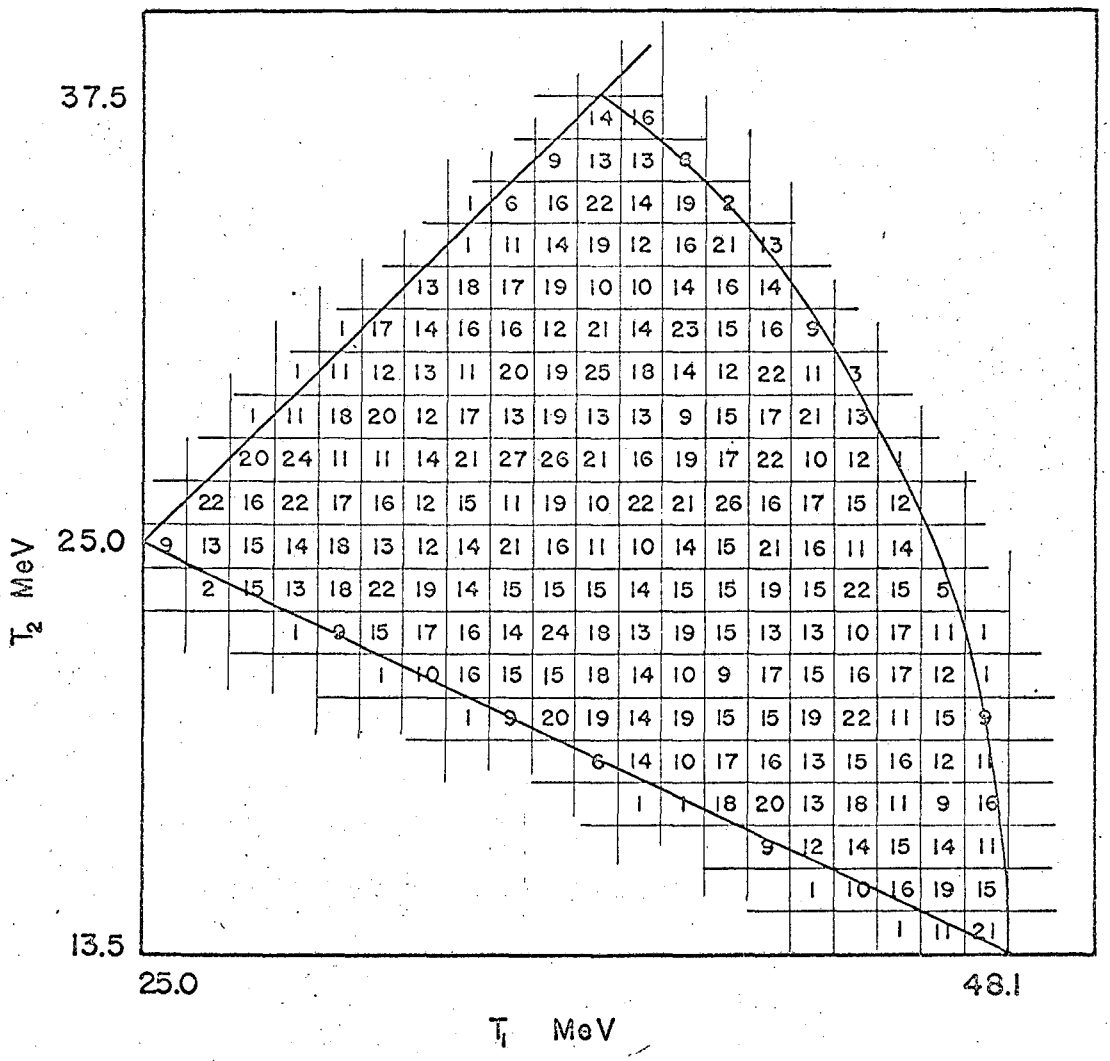

Figure 9

TABLE II. Results of τ analysis.

Matrix element and most probable values for parameters from maximum likelihood calculation.	$\frac{\text{likelihood}}{\text{resonance likelihood}}$	Chi-square probability
Resonance $M_\sigma = 348 \pm 2$ $\Gamma_\sigma = 50 \pm 11$	1	.4%
Variable width resonance $M_\sigma = 357 \pm 5$ $\Gamma_o = 55 \pm 16$	1	---
Quadratic matrix element $M = 1+a(s_3-s_o) + b(s_3-s_o)^2$ $2b + a^2 = (-1.8 \pm .5)\times 10^{-5}$	$\frac{1}{7200}$	---

In order to determine the value of b the data of McKenna et al.[1] were used to obtain a measure of the linear term, a. A chi-square fit to these data using a matrix element of the form $M = 1 + a(s_3-s_o)$ gives the value $a = .093 \pm .027$ with a chi square of 17.4 while the expected chi square value was 29. Using this value for a we have

$$b = -.004 \pm .003$$

$$M_\tau = 1 + (.093 \pm .27)(s_3-s_o) + (-.004 \pm .003)(s_3-s_o)^2.$$

These results may be stated as follows: Since the quadratic term in the Daltiz plot density is small and the density is proportional to the matrix element squared the existence of a linear term in the matrix element implies there must be higher order terms also. The fitting

programs used were tested with a Monte Carlo generated sample of τ events. The likelihood program and the chi-square program correctly reproduced the original generation parameters and the chi square value was 140 with an expected value of 135.

Several other forms of the matrix element for τ decay were tried in an attempt to find a form which gave a better fit. The forms tried were the scattering length parametrization of Khuri and Treiman,[7] a matrix element suggested by Zemach[10] and a combination resonance plus phase space. In each case the best-fit parameters led to a smaller chi-square probability of fit than the other hypotheses tested.

Earlier analyses of τ decay have used a squared matrix element of the form $M_\tau^2 = 1 + a(s_3 - s_o)$. This leads to a constant density in the charge-undetermined Dalitz plot. For our τ^+ data, the ratio of constant-density likelihood to resonance likelihood is 10^{-9}. This fact clearly indicates the necessity of nonlinear terms in the square of the matrix element.

IV. DISCUSSION

When one considers the recent experimental developments involving K meson decay, which include violation of time reversal invariance[16-18] and unexplained energy and angular correlation,[19-20] the fact that none of the various matrix elements used to fit τ^+ decay provided a fit with better than a 1% probability certainly indicates a need for additional theoretical consideration of these decays and may also provide a possible clue to the form of these considerations.

The lack of a good fit to the τ^+ charge-undetermined Dalitz plot density, when compared with the relatively good fits obtained earlier[1-4] for a one-axis projection of the Dalitz plot, indicates that vital information may be lost in making this projection. Thus it is possible that an experimental determination of the two dimensional Dalitz plot density for τ' decay would contribute new and useful information.

The data of this experiment provide a good test of the "σ" resonance hypothesis.[5] The τ^+ and τ'^+ best-fit values for the mass agree quite well. However, the widths are several standard deviations apart and in the case of τ^+ decay the fit was very poor. This is evidence that the resonance theory provides a poor description of $K^+_{3\pi}$ decay in its present form. Considering the excellent agreement of the mass values, one may speculate that there is resonance behavior and that the data will contribute to the formulation of the correct energy dependence of the width in this region, for this energy dependence is also an unsettled question.[15]

In order to consider the applicability of the "σ" resonance

hypothesis it is necessary to consider experimental data from several sources. A study of the energy spectrum of the reaction $\eta \rightarrow \pi^+\pi^-\pi^o$ [22] produced best fit parameters $M_\sigma = 392 \pm 9$ and $\Gamma_\sigma = 88 \pm 15$. Again the values are not consistant. A study of K_{e4} decay,[23] where there are only two pions available to interact, revealed that the di-pion mass spectrum was very close to phase space. This appears to be inconsistent with the resonance parameters determined from our τ^+ data. Finally a work in progress[24] which combines the energy spectra and branching ratios from both η and K decay data indicates the resonance hypothesis must be modified by adding a non-resonant background with arbitrary amplitude and phase (i.e., a 4 parameter fit) in order to be consistant with these data. In view of this evidence it may be said that the K-decay data are not satisfactorily explained by the existence of an $I = 0$, $J^P = 0^+$ π-π resonance.

ACKNOWLEDGMENTS

I would like to thank Professor Walter H. Barkas and Dr. Zack Osborne for their guidance and suggestions concerning all phases of this work.

My thanks also to the scientific data analysts of the Barkas Physics Research Group for their excellent work in taking these data, in particular I must mention Jim Webber and Peter Lindstrom who offered many creative and helpful suggestions. Sincere thanks to Carol Pierson who, through the years, has eased the weight of innumerable administrative details.

This work could have never been done without the help and encouragement of my wife Penelope. Numerous communications with Thom Pari and Bert Carter III cleared up many points of confusion in the early stages of this work.

This work was done under the auspices of the U. S. Atomic Energy Commission.

APPENDICES

A. Analysis of Scanning Efficiency

1. τ

In order to determine the efficiency of finding τ events a second independent scan was made of all the area. The efficiency was calculated as follows. Let N_1 and N_2 be the number of events found during the first and second scans, respectively. Let N be the actual number of events in the area. Then the efficiencies of the two scanners are

$$\epsilon_1 = N_1/N \qquad \epsilon_2 = N_2/N .$$

If the scans are independent then

$$\epsilon_1\epsilon_2 = N_{12}/N = N_1N_2/N^2 ,$$

where N_{12} = the number of events common to both scans.

These three equations may be solved for N, ϵ_1 and ϵ_2. The solutions are

$$N = \frac{N_1N_2}{N_{12}} \qquad \epsilon_1 = \frac{N_{12}}{N_2} \qquad \epsilon_2 = \frac{N_{12}}{N_1} .$$

The total efficiency is then

$$\epsilon = \epsilon_1 + (1 - \epsilon_1)\epsilon_2 .$$

This method was applied to the distributions of largest energy, largest included angle between secondaries and direction of normal to decay plane. Table 3 lists these efficiencies. The total efficiencies were found to be between 97% and 100% and constant over the distributions.

TABLE III. τ scanning efficiencies.

$\cos\theta_{max}$ Interval	Efficiency	E_{max} Interval	Efficiency	$n \cdot z$ * Interval	Efficiency
-1.0 to -.95	98.9	163 to 166	100.0	-1.0 to -.8	99.3
-0.95 to -.90	99.3	166 to 169	99.2	-0.8 to -.6	99.5
-0.90 to -.85	99.3	169 to 172	99.3	-0.6 to -.5	99.2
-0.85 to -.80	99.1	172 to 175	99.1	-0.4 to -.2	98.7
-0.80 to -.75	99.4	175 to 178	99.4	-0.2 to 0.0	99.3
-0.75 to -.70	99.5	178 to 181	98.8	0.0 to 0.2	99.2
-0.70 to -.65	99.6	181 to 184	99.5	0.2 to 0.4	98.9
-0.65 to -.60	99.2	184 to 187	99.0	0.4 to 0.6	99.2
-0.60 to 0.55	97.7	187 to 190	99.5	0.6 to 0.8	99.4
-0.55 to -.50	100.0			0.8 to 1.0	99.3

* The normal was defined by the cross product of the highest energy prong direction into the lowest energy prong direction.

2. τ'

A bias-free sample of τ' events with grain density $\geq 2 \times$ minimum would provide the energy spectrum up to 37 MeV. Since an actual grain count was not made we expected to lose events near the $2 \times$ minimum region. Comparison with an earlier sample of τ' events which were grain counted showed that above 25 MeV the efficiency decreased. Therefore we consider the region 0-20 MeV.

In order to test the energy variation of the efficiency, split the distribution into 5 MeV intervals and consider the distribution of dip angle cosines of the events in each energy interval. Let a_i represent the number of events in the i^{th} dip angle cosine interval. A measure of the deviation from isotropy is the quantity

$$\epsilon = \left(\frac{\langle a \rangle}{\langle a^2 \rangle - \langle a \rangle^2} \right)^{\frac{1}{2}} .$$

If the distribution is isotropic then $\langle a^2 \rangle - \langle a \rangle^2 = \langle a \rangle$ or $\epsilon = 1$. The variation of ϵ over the 0-20 MeV range is quite small which implies the efficiency is constant over this energy region. Table 4 gives the value of ϵ for each energy interval. The values of ϵ differ from unity due to loss of events at large dip angles, this of course does not bias the energy spectrum. Table V gives the dip angle distribution for the four energy intervals. Figure 10 shows the original and corrected spectra. In both Table 4 and Fig. 10 the corrected spectrum is normalized to the original number of events to emphasize the variation of the efficiency which is the prime consideration here.

Table IV. τ' scanning efficiency

Energy Interval	ϵ	Observed number of events	Corrected number of events
0 - 5 MeV	.76	44	44.9
5 - 10 MeV	.75	89	92.5
10 - 15 MeV	.81	113	107.8
15 - 20 MeV	.77	131	131.8

Table V. Dip angle distribution

Dip cosine interval	0-5 MeV	5-10 MeV	10-15 MeV	15-20 MeV
-1.0 to -0.8	1	5	7	9
-0.8 to -0.6	4	4	9	10
-0.6 to -0.4	2	12	15	9
-0.4 to -0.2	5	6	14	19
-0.2 to -0.0	7	15	6	16
-0.0 to 0.2	7	12	10	7
0.2 to 0.4	3	8	16	20
0.4 to 0.6	10	11	18	16
0.6 to 0.8	4	13	12	17
0.8 to 1.0	1	3	5	8

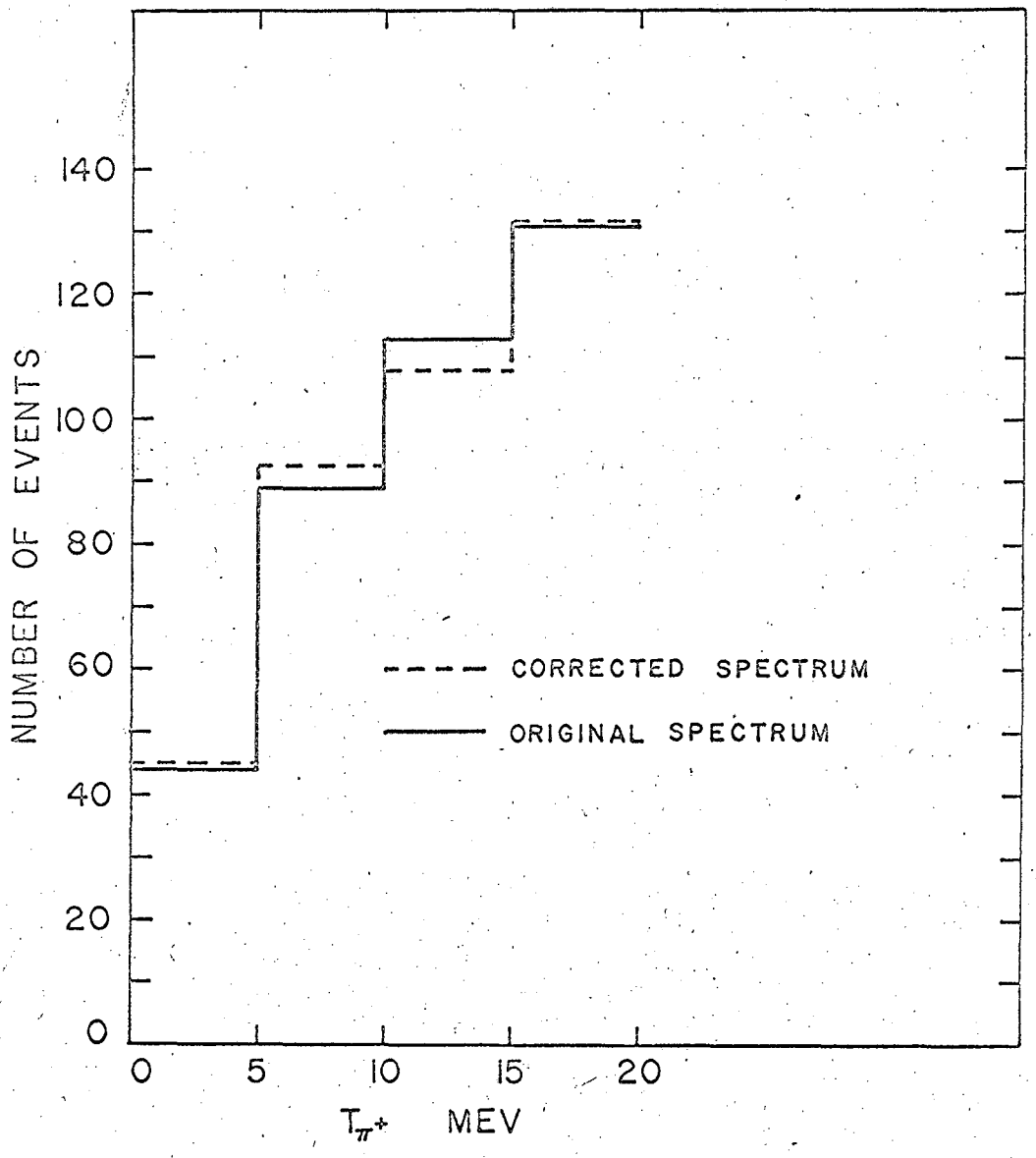
NUMBER OF EVENTS
140
120
100
80
60
40
20
0
0
5
10
15
20
T_{π^+} MEV
CORRECTED SPECTRUM
ORIGINAL SPECTRUM

Figure 10

B. Fitting Procedure

Let (f_{i1}, f_{i2}, f_{i3}) be the coordinates of the point nearest to the K-decay vertex on the i^{th} track and (g_{i1}, g_{i2}, g_{i3}) be the coordinates of the second point on the i^{th} track. These points are the measured coordinates shown in Fig. 11. Define the lengths x_i^m as,

$$x_1^m = g_{11} - f_{11} \quad x_2^m = g_{12} - f_{12} \quad x_3^m = (g_{13} - f_{13})S$$

$$x_4^m = g_{21} - f_{21} \quad x_5^m = g_{22} - f_{22} \quad x_6^m = (g_{23} - f_{23})S$$

$$x_7^m = g_{31} - f_{31} \quad x_8^m = g_{32} - f_{32} \quad x_9^m = (g_{33} - f_{33})S$$

Here, S, the shrinkage factor of the emulsion at the time of measurement, is needed as $x^m_{i=3,6,9}$ are the vertical directions.

Conservation of momentum requires:

$$\frac{P_1 x_1^m}{\ell_1} + \frac{P_2 x_4^m}{\ell_2} + \frac{P_3 x_7^m}{\ell_3} = 0 \qquad (1)$$

$$\frac{P_1 x_2^m}{\ell_1} + \frac{P_2 x_5^m}{\ell_2} + \frac{P_3 x_8^m}{\ell_3} = 0 \qquad (2)$$

$$\frac{P_1 x_3^m}{\ell_1} + \frac{P_2 x_6^m}{\ell_2} + \frac{P_3 x_9^m}{\ell_3} = 0 \qquad (3)$$

$$(P_1^2 + m^2)^{\frac{1}{2}} + (P_2^2 + m^2)^{\frac{1}{2}} + (P_3^2 + m^2)^{\frac{1}{2}} - M = 0 \qquad (4)$$

where P_i = momentum magnitude of the i^{th} track, $\ell_i = \left(\sum_{j=3i-2}^{3i} (x_j^m)^2 \right)^{\frac{1}{2}}$ the length between measured points on th i^{th} track, m = pion mass and M = kaon mass.

The quantity chi square is defined as follows

$$\chi^2 \equiv \sum_{\substack{i=1 \\ j=1}}^{9} (x_i - x_i^m)\, G_{ij}\, (x_j - x_j^m) \quad .$$

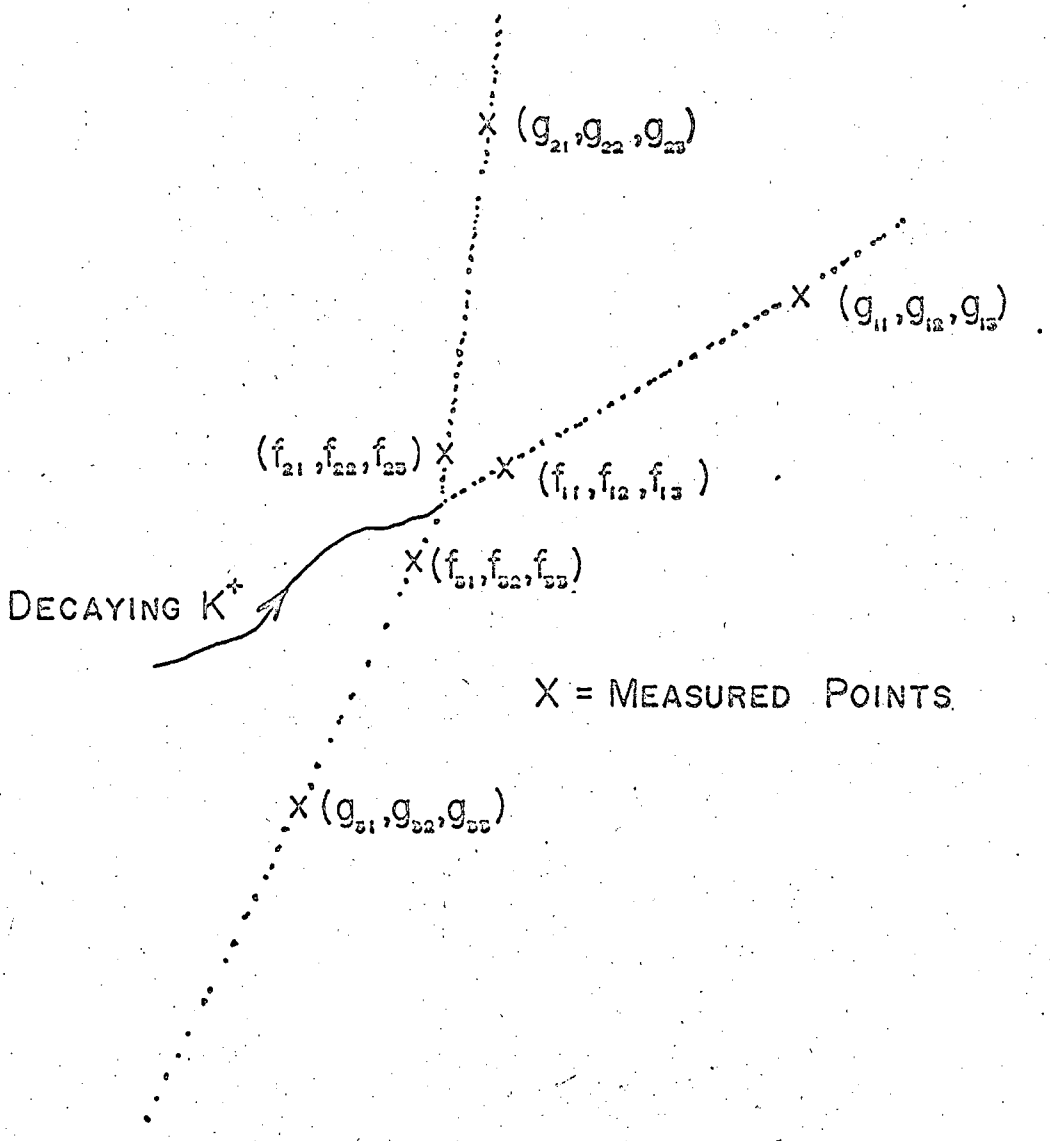
(g_{21}, g_{22}, g_{23})
(g_{11}, g_{12}, g_{13})
(f_{21}, f_{22}, f_{23})
(f_{11}, f_{12}, f_{13})
(f_{01}, f_{02}, f_{03})
DECAYING K^+
X = MEASURED POINTS
(g_{01}, g_{02}, g_{03})

Figure 11

Here, the x_i are the computed values of the lengths satisfying the restrictions of equations 1-4. Also $G^{-1}_{ij} = \langle \delta x_i \delta x_j \rangle$, the matrix of input errors. If one assumes there is no correlation between measurement errors on separate tracks then G^{-1} reduces to

$$G^{-1} = \begin{pmatrix} g_1 & 0 & 0 \\ 0 & g_2 & 0 \\ 0 & 0 & g_3 \end{pmatrix}$$

where g_i is a 3-by-3 error matrix for the i^{th} track. Tests performed with the microscope used showed there was negligible correlation between measurements along different axes, therefore the g_i are diagonal. The final form for g_i in units of μ^2 was

$$g_i = \begin{pmatrix} 2\sigma_x^2 & 0 & 0 \\ 0 & 2\sigma_y^2 & 0 \\ 0 & 0 & (\delta S \cdot x_{3i})^2 + S^2\sigma_z^2 \end{pmatrix}$$

where σ_S is .01S, and σ_x, σ_y, σ_z = .5μ.

The Lagrange multiplier method was used and equation 3 was taken as the constraint. The quantity minimized was

$$M = \sum_{\substack{i=1 \\ j=1}}^{9} (x_i - x_i^m)\, G_{ig}\, (x_g - x_g^m) + 2aF(x)$$

where $F(x) = \sum_{i=1}^{3} \frac{P_i x_{3i}}{\ell_i}$ and a is the Lagrange multiplier. From this point the calculation proceeds exactly as shown in the article by Berge, Solmitz and Taft[11]--an iterative procedure is set up and the minimum of M is approached.

Figure 12 shows the distribution of chi squares. The scale of the ordinate is constructed so that a chi-square distribution with one degree of freedom and correct input errors (a = 1) will fall on the straight line labeled a = 1. As Fig. 12 shows, the resulting χ^2 distribution is linear and indicates a slight overestimation of input errors. The standard method of scaling the propagated errors[14] was used as the time and cost required for recomputation would have been excessive.

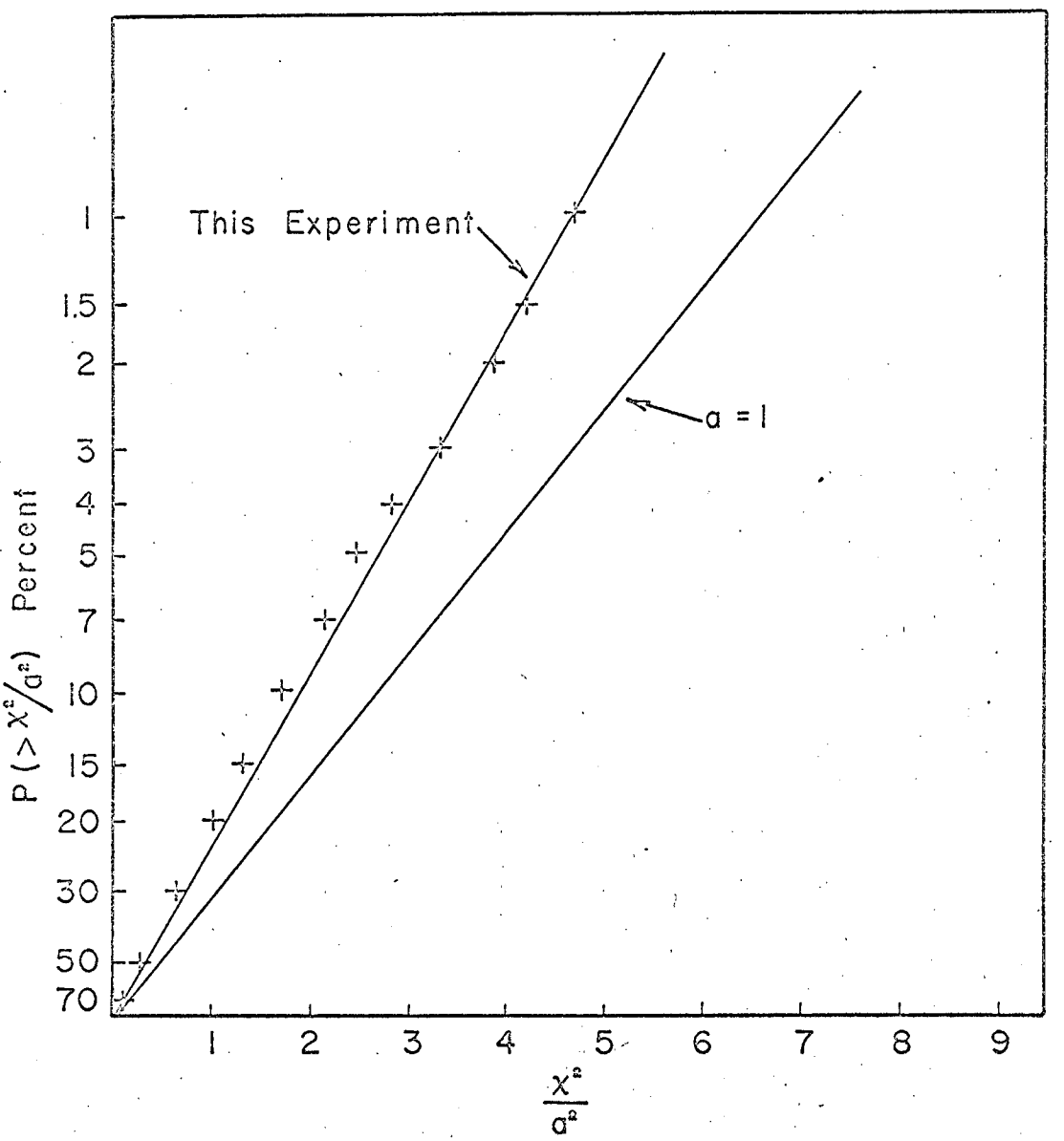
This Experiment
a = 1
P (> χ²/a²) Percent
1
1.5
2
3
4
5
7
10
15
20
30
50
70
1
2
3
4
5
6
7
8
9
χ²/a²

Figure 12

C. Matrix Elements

1. τ' decay

Brown and Singer[5] give the following matrix element assuming a resonant reaction between the uncharged pions

$$M = \frac{1}{(p_K - p_+)^2 - (M_\sigma - \frac{i\Gamma_\sigma}{2})^2} .$$

Here p_K is the K^+ 4-momentum, p_+ is the π^+ 4-momentum, M_σ is the mass of the resonance and Γ_σ is the width of the resonance.

Jackson[15] has pointed out that the energy dependence of Γ_σ may be important in evaluating resonance parameters. This possibility has been examined in connection with the τ' and τ data furnished by this experiment. The energy dependence used was $\Gamma_\sigma = \Gamma_o q/q_o$ where q = relative momentum of the resonance decay products in the resonance rest system and $q_o^2 = (\frac{M_\sigma}{2})^2 - m_{\pi o}^2$, the relative momentum when the resonance rest mass is at the central value.

Another matrix element tested was simply the first few terms of a power series expansion of the matrix element. Let $s_i = (p_K - p_i)^2$, where p_i is the 4-momentum of the i^{th} pion and $s_o = (s_1 + s_2 + s_3)/3$. M is then expressed in powers of $(s_3 - s_o)$ where the subscript 3 refers to the odd pion.

$$M = 1 + a(s_3 - s_o) + b(s_3 - s_o)^2 + \ldots$$

Of course terms of the form $(s_1 - s_2)^2$ are possible; however, we have no measure of the values of s_1 and s_2.

2. τ decay

Again both forms of resonance matrix element were used. Since there are two possible resonant pion combinations the amplitude has the form

$$M = \frac{1}{(p_K - p_{1+})^2 - (M_\sigma - \frac{i\Gamma_\sigma}{2})^2} + \frac{1}{(p_K - p_{2+})^2 - (M_\sigma - \frac{i\Gamma_\sigma}{2})^2}$$

where p_{1+}, p_{2+} refer to the 4-momenta of the π^+ decay products. The resultant density is ~~of course~~

$$\rho \alpha M(p_1, p_2)\, M^*(p_1, p_2) + M(p_2, p_3)\, M^*(p_2, p_3) + M(p_3, p_1)\, M^*(p_3, p_1).$$

The following power series expansion of the matrix element was used

$$M = 1 + a\,(s_3 - s_o) + b\,(s_3 - s_o)^2 + c\,(s_1 - s_o)(s_2 - s_o).$$

In this case the resultant density becomes

$$\rho \alpha 3 + (a+a^*) \sum_{i=1}^{i=3} (s_i - s_o) + (b+b^*+aa^*) \sum_{i=1}^{i=3} (s_i - s_o)^2$$

$$+ (c+c^*)((s_1-s_o)(s_2-s_o) + (s_2-s_o)(s_3-s_o) + (s_3-s_o)(s_1-s_o))$$

$$+ (ab^*+ba^*) \sum_{i=1}^{i=3} (s_i - s_o)^3 + 3(ac^*+ca^*)(s_1-s_o)(s_2-s_o)(s_3-s_o)$$

$$+ bb^* \sum_{i=1}^{i=3} (s_i - s_o)^4 + (b^*c+c^*b)(s_1-s_o)(s_2-s_o)(s_3-s_o) \sum_{i=1}^{i=3} (s_i - s_o)$$

$$+ cc^*((s_1-s_o)^2(s_2-s_o)^2 + (s_2-s_o)^2(s_3-s_o)^2 + (s_3-s_o)^2(s_1-s_o)^2).$$

However

$$\sum_{i=1}^{i=3} (s_i - s_o) = 0$$

and $$(s_1-s_o)^2(s_1-s_o)^2 + (s_2-s_o)^2(s_3-s_o)^2 + (s_3-s_o)^2(s_1-s_o)^2$$

$$= ((s_1-s_o)(s_2-s_o) + (s_2-s_o)(s_3-s_o) + (s_3-s_o)(s_1-s_o))^2$$

so we have

$$\rho \alpha 3 + (b+b^*+aa^*)\sum_{i=1}^{i=3}(s_i-s_o)^2 + (c+c^*)((s_1-s_o)(s_2-s_o) + (s_2-s_o)(s_3-s_o)$$

$$+ (s_3-s_o)(s_1-s_o)) + (ab^*+ba^*)\sum_{i=1}^{i=3}(s_i-s_o)^3 + 3(ac^*+ca^*)(s_1-s_o)(s_2-s_o)(s_3-s_o)$$

$$+ bb^*\sum_{i=1}^{i=3}(s_i-s_o)^4 + cc^*((s_1-s_o)(s_2-s_o) + (s_2-s_o)(s_3-s_o) + (s_3-s_o)(s_1-s_o))^2$$

If we keep only terms up to quadratic in the variables s_i we have

$$\rho \alpha 3 + (b+b^*+aa^*)\sum_{i=1}^{i=3}(s_i-s_o)^2 + (c+c^*)((s_1-s_o)(s_2-s_o) + (s_2-s_o)(s_3-s_o)$$

$$+ (s_3-s_o)(s_1-s_o)).$$

Thus, using this method, we may evaluate $(b+b^*+aa^*)$ and $(c+c^*)$. If all coefficients are assumed real then, assuming an earlier value[1] for a, it is possible to determine b and c.

D. Statistical Methods

1. Likelihood Methods

Let $f(x,y,p_j)$ be a distribution function for the experimental variables x and y where p_j are certain input parameters. The likelihood function

$$L(p_j) = \prod_{i=1}^{n} f(x_i, y_i, p_j)$$

is the joint probability density of getting a particular experimental result, $(x_1 y_1)$, ..., (x_n, y_n) assuming $f(x, y, p_j)$ is the true normalized distribution function. The most probable value of each p_j, found by maximizing $L(p_j)$, is called the maximum-likelihood solution p_j^*. In practice this maximum-likelihood solution is found by maximizing the log of $L(p_j)$. If the likelihood function is Gaussianlike in the region $p_j \approx p_j^*$ the error matrix for the p_j is

$$\overline{(p_\ell - p_\ell^*)(p_i - p_i^*)} = \left(- \frac{\partial^2 \ell n L(p_j)}{\partial p_\ell \, \partial p_i} \right)^{-1}$$

A likelihood ratio is useful for choosing between different forms for the distribution function. If $g(x, y, a)$ and $f(x, y, b)$ are two distribution functions then

$$R = \prod_{i=1}^{n} \frac{f(x_i, y_i, b)}{g(x_i, y_i, a)}$$

is the likelihood ratio. R is the probability of getting the set of n events assuming f is true divided by the probability of getting the n events if g is true, or simply the betting odds of f against g.

2. Chi-square methods

Assume we have n measurements at the points $x_1, \ldots, x_n$ and the results are $(y_1 \pm \sigma_1), \ldots, (y_n \pm \sigma_n)$ and we have a distribution function $y(x, p_j)$ then chi-square is defined as

$$\chi^2(p_j) = \sum_{i=1}^{n} \frac{(y_i - y(x_i, p_j))^2}{\sigma^2}$$

The best fit parameters p_j^* are found by minimizing $\chi^2(p_j)$ with respect to the p_j. If the $\chi^2(p_j)$ function is Gaussianlike in the region of $p_j \approx p_j^*$ then the error matrix is

$$\overline{(p_i - p_i^*)(p_\ell - p_\ell^*)} = \left(\tfrac{1}{2} \frac{\partial^2 \chi^2}{\partial p_i \partial p_\ell} \right)^{-1} .$$

3. Goodness-of-fit

It is possible to calculate the expected distribution of χ^2 as a function of n-M where M is the number of parameters p_j used in the distribution function. For given n-M (called "degrees of freedom") there are tables of the probability of exceeding a given value of χ^2 given in the Handbook of Chemistry and Physics and other common mathematical tables.

This probability is generally called the chi-square probability for a given hypothesis and is used to provide a test of how well a particular hypothesis fits experimental data.

4. Example of χ^2 calculation

In the case of τ decay the Dalitz plot was partitioned into bins by a grid of an appropriate number of divisions in each direction. Each bin contained a number of events y_i with a standard deviation $\sigma_i = (y_i)^{\frac{1}{2}}$. The value of the distribution function for a bin was just the integral

of the squared matrix element being tested over the energy region of the bin. The corresponding value of χ^2 is

$$\chi^2 = \sum_{\text{All bins}} \frac{(y_i - N_i)^2}{N_i}$$

where N_i = expected number of events in the i^{th} bin.

A function minimizing routine was used to find the parameters which gave the minimum value for χ^2.

REFERENCES

1. S. McKenna, S. Natali, M. O'Connell, J. Tietge, N. C. Varshneya, A study of 540 τ-Meson Decays, Nuovo Cimento X, 763 (1958).
2. M. Baldo-Ceolin, A. Bonetti, W. D. B. Greening, S. Limentani, M. Merlin and G. Vanderhaeghe, An Analysis of 419 τ-Meson Decays, Nuovo Cimento VI, 84 (1957).
3. George E. Kalmus, Anne Kernan, Robert T. Pu, Wilson M. Powell, and Richard Dowd, Energy Spectrum of π^+ in $K^+ \rightarrow \pi^+\pi^o\pi^o$ Decay, Phys. Rev. Letters 13, 99 (1964).
4. G. Giacomelli, D. Monti, G. Quareni, A. Quareni-Vignudelli, W. Puschel, J. Tietge, Study of 224 τ'^+ Decays, Physics Letters 3, 346 (1963).
5. Laurie M. Brown and Paul Singer, Three Pion Decay Modes of Eta and K Mesons and a Possible New Resonance, Phys. Rev. 133, B812 (1964).
6. E. Lomon and S. Morris, The Pion-Pion Interaction in τ Decay, Annals of Physics 13, 359 (1961).
7. N. N. Khuri and S. B. Treiman, Pion-Pion Scattering and $K^{\pm} \rightarrow 3\pi$ Decay, Phys. Rev. 119, 1115 (1960).
8. I. J. R. Aitchison, A. Dispersion Theory Model of Three Body Production and Decay Processes, Phys. Rev. 137, B1070 (1965).
9. Steven Weinberg, New Test for $\Delta I = 1/2$ in K^+ Decay, Phys. Rev. Letters 4, 87 (1960).
10. Charles Zemach, Three-Pion Decays of Unstable Particles, Phys. Rev. 133, B1201 (1964).
11. J. Peter Berge, F. T. Solmitz and Horace D. Taft, Kinematical Analysis of Interaction Vertices from Bubble Chamber Data, Rev. Sci. Instr. 32, 538 (1961).

12. Douglas E. Greiner, W. Z. Osborne, and Walter H. Barkas, An Example of $K_{\mu 4}$ Decay in Emulsion, Phys. Rev. Letters 13, 284 (1964).

13. Arthur H. Rosenfeld, Angela Barbaro-Galtieri, Walter H. Barkas, Pierre L. Bastien, Janos Kirz and Matts Roos, Data on Elementary Particles and Resonant States, Rev. of Mod. Phys. 36, 977 (1964).

14. William E. Humphrey and Arthur H. Rosenfeld, Analysis of Bubble Chamber Data, Ann. Rev. Nucl. Sci. 13, 103 (1963).

15. J. D. Jackson, Remarks on the Pheonomenological Analysis of Resonances, Nuovo Cimento 34, 1644 (1964).

16. J. M. Christenson, J. W. Cronin, V. L. Fitch, and R. Turlay, Evidence for the 2π Decay of the K_2^o Meson, Phys. Rev. Letters 13, 138 (1964).

17. W. Galbraith, G. Manning, A. E. Taylor, B. D. Jones, J. Malos, A. Astbury, N. H. Lipman and T. G. Walker, Two-Pion Decay of the K_2^o Meson, Phys. Rev. Letters 14, 383 (1965).

18. Jared A. Anderson, Frank S. Crawford, Jr., Robert L. Golden, Donald Stern, Thomas O. Binford, and V. Gordon Lind, CP-Nonconserving Decay $K_1^o \rightarrow \pi^+ + \pi^- + \pi^o$, Phys. Rev. Letters 14, 475 (1965).

19. W. Z. Osborne, Search for Evidence of a Pion Memory, Bull. Am. Phys. Soc. 11, 168 (1965).

20. G. B. Cvijanovich and E. A. Jeannet and E. C. G. Sudarshan, CP Invariance in Weak Interactions and the Pion Decay Asymmetry, Phys. Rev. Letters 14, 117 (1965).

21. G. B. Cvijanovich and E. A. Jeannet, Helv. Phys. Acta 37, 211 (1964).

22. F. S. Crawford, Jr., R. A. Grossman, L. J. Lloyd, Leroy R. Price, and E. C. Fowler, Final State Interactions in the Decay $\eta^o \rightarrow 3\pi$, Phys. Rev. Letters 11, 564 (1963), see also Erratum, Phys. Rev. Letters 13, 421 (1964).

23. R. W. Birge, R. P. Ely, G. Giadel, G. E. Kalmus, A. Kernan, et al., University of California Radiation Laboratory Report, UCRL-11549, (to be published). Also private communications with G. E. Kalmus.

24. Private communications with Leroy R. Price, University of California Radiation Laboratory. See also Claude Kacser, Paul Singer and Tran N. Truong, Study of K_{e4} Decays, Phys. Rev. 137, B1605 (1965).

25. Jay Orear, Notes on Statistics for Physicists, University of California Radiation Laboratory Report, UCRL-8417 August 13, 1958.

FIGURE CAPTIONS

Fig. 1 A photograph of the emulsion stack used in this experiment. The K^+ beam entered through the brass plate at the left. The stack clamp design allowed all emulsion edges to be machined flat.

Fig. 2 Experimental arrangement. M_1 and M_2 are bending magnets, Q_1 is a quadrupole focusing magnet and S_1 is a velocity selector.

Fig. 3 A typical plate showing alignment tab and reinforcement strips.

Fig. 4 The one millimeter coordinate grid which was contact printed in an identical position on each pellicle to provide a coordinate frame visible in each field of view.

Fig. 5 Several τ decay configurations.

a. Approximately equal energy prongs and flat decay plane.

b. An event where the decay plane is not horizontal.

c. Two prongs of this event are approximately collinear.

Fig. 6 Momentum balance tests.

a. An event which can conserve momentum.

b. All prongs point into one hemisphere thus momentum cannot balance.

c. The parallelepiped whose volume must be zero for τ decay.

Fig. 7 τ' spectrum divided by phase space, points above 10 MeV are from reference 3. The curves are the best fit for resonance, quadratic and linear matrix elements.

Fig. 8 Dalitz plot showing the six possible locations for one event. Sextant I was used in fitting calculations.

Fig. 9 The experimental distribution of τ events in sextant I of the Dalitz plot.

Fig. 10 τ' spectrum between 0 and 20 MeV.

Fig. 11 A τ event with measured points indicated.

Fig. 12 The distribution of chi squares.